

Validation of the DLR dual stream jet noise test rig at the Aeroacoustic Wind Tunnel Braunschweig

Christian Jente¹, Peer Böhning²

¹ Deutsches Zentrum für Luft- und Raumfahrt e.V., 38108 Braunschweig, email: christian.jente@dlr.de

² Rolls-Royce Deutschland Ltd & Co KG, Dahlewitz, 15827 Blankenfelde-Mahlow

Introduction

DLR Braunschweig conducted multiple jet installation noise tests between 2019 and 2024, among others in the projects FOTEKO, DJINN [7], and MUTE – but how good is the test data and what are the physical operating limits in the Aeroacoustic Wind Tunnel Braunschweig (AWB)?

Rather large models (jet diameters $D_j = \text{Ø}80\text{mm}$ to $\text{Ø}95\text{mm}$) were fit into the small AWB test room, resulting in close microphone positions of $R_{\text{mic}}/D_j \sim 20$. However, the recommended microphone distance for testing isolated jet noise without the need for source correction is $R_{\text{mic}}/D_j = 100$ [1]. Hence, DLR-BS was put into a situation to study the jet's source distribution just to make reasonable far-field projections and to qualify their isolated and installed jet noise test data.



Figure 1: Static jet noise test setup for validation of the dual stream engine models at AWB, July 2024. Instrumentation is setup as a close listener $R_{\text{mic}}/D_j = 17 \dots 50$.

Test facility, model and instrumentation for small test room / large model

The challenge of measuring models that are too large in relation to the test room is the violation of the geometric far-field distance and perhaps insufficient polar angle coverage of the far-field microphones. This was countered by the following innovations (Figures 1 and 2):

1. the development of an AWB microphone arc incl. 20° and 30° microphones which allows clean analysis of rear-arc jet noise spectra, so-called F-noise by Tam [4].
2. by positioning the microphone around the low-frequency source point. It was initially assumed to be fixed at $X=7 \cdot D_j$ [2], but also controlled by source localisation using AWB's $96 \times \frac{1}{2}$ " LinearX microphone array in the $\Theta=90^\circ$ position.

2 Fixed measurement reference point $\Theta=90^\circ$

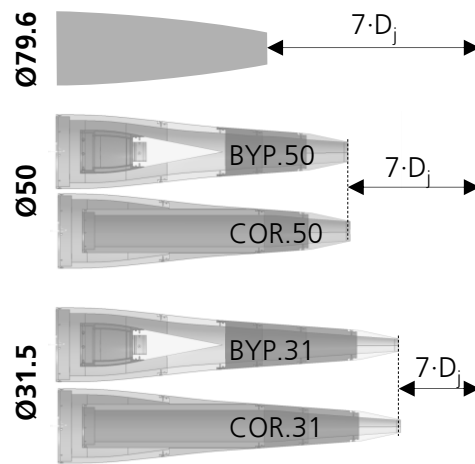


Figure 2: Engine model adapters designed for a fixed measurement reference point $7 \cdot D_j$ downstream the engine exit. Bypass and Core single stream models were used for individual duct analysis.

Jet noise source peak analysis – Is $7 \cdot D_j$ good?

The source map of single stream jet noise (Figure 3) shows a low-frequency source point (1) around $X=7 \cdot D_j$. The position fits exactly at $M_j=0.7$, but shifts slightly by $\pm 1 \cdot D_j$ depending on the Mach number (Figure 4).

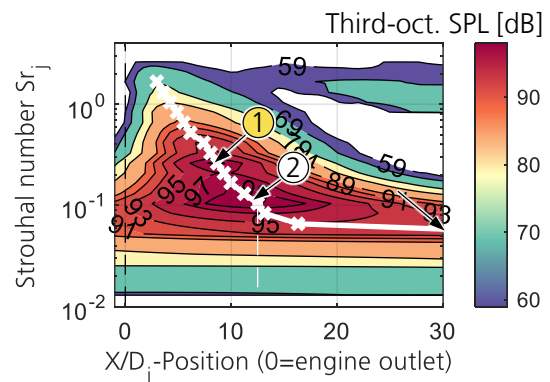


Figure 3: Jet noise source distribution along jet axis at $M_j=0.86$ for $\text{Ø}31.5\text{mm}$ jet, array direction = 90° (see Figure 1), frequency resolution: third-octaves, containing not only one, but two low-frequency peaks

Much more exciting than the slight shift of peak 1 is the surprising discovery of an at least equally relevant second low-frequency source point at $X=10 \cdot D_j$ in Figure 3.

Both of the peaks ($He=0.09$ and $He=0.23$) differ in their velocity scaling exponent by 2. While peak 2 is slightly larger in gain for low speed (Figure 4), peak 1 outgrows peak 2 close to sonic jet operations.

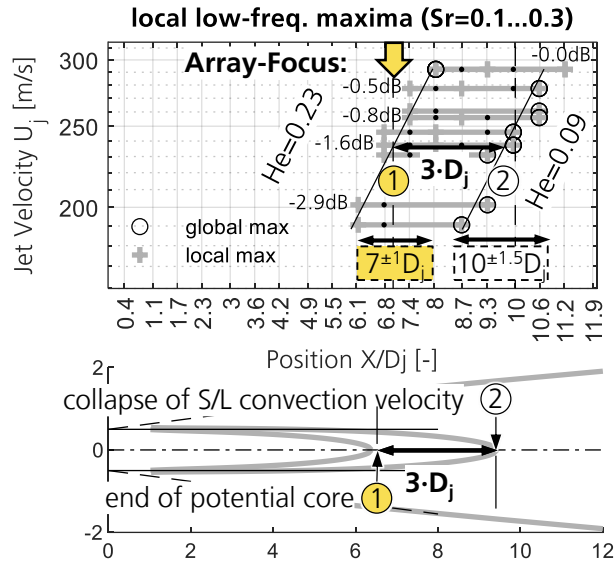


Figure 4: X-Position of jet noise source maxima by jet velocity and jet geometry

Moreover, the two points are distanced by $\Delta X=3 \cdot D_j$ which (Figure 4) roughly represents the distance between the collapse of the jet potential core and the jet's near field shear layer (a thin mixing layer centered around the nozzle lip line). This indicates two different source mechanisms as postulated in the literature [4]:

The entire distributed source around peak 2 composes the characteristic **forward-to-overhead jet noise** (called G-noise by Tam) with its wide shape function (Figure 8). Frequencies depend on Strouhal number. The historically established choice of $Sr_j=f \cdot D_j/U_j$ allows for good collapse of forward-overhead jet noise, but also for the flight effect [3] (which is oddly surprising and non-intuitive, since the flight speed U_∞ is ignored).

The characteristic **rear-arc jet noise shape function**, F-noise, is rather steep (Figure 8) and can be measured best at high subsonic operations. It is related to peak 1 in the source maps. The measured frequency peaks of the third-octave sound pressure spectra do not follow a Strouhal analogy.

The shape functions of the intermediate polar angles of 30° - 70° are a bit more complicated to model, since they are a superposition of the F- and G-shapes: The F-shape controls the peak, while the G-shape the wider shape. This leads to the state of an overall uncommon peak frequency dependency along the overall arc.

Static jet noise source distribution

The maximal gain X-position for each frequency (white line in Figure 3) is extracted for various jet Mach numbers between 0.6 and 0.9 and nozzle diameters. The X-values are cut off at two significant positions:

1. The minimal X-position is close to or at the engine exit. The detection is limited by the high frequency capabilities of the array and evaluation algorithm.
2. The max(X)-position is the peak SPL position. It shifts depending on Mach number (see also [6]). This position is the true reference point for the jet noise source. It defines the most accurate source origin.

The individual source distribution functions collapse well when choosing the Strouhal number as non-dimensional frequency (Figure 5).

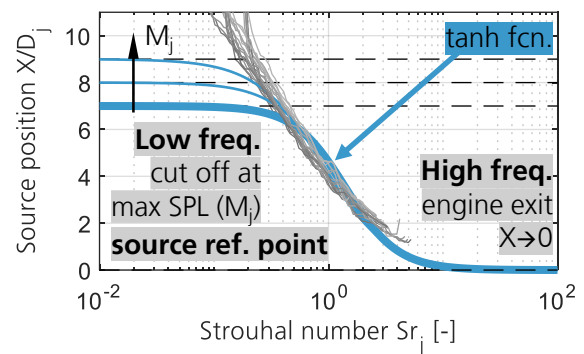


Figure 5: Source distribution function of single stream jet noise, collapse for 3 nozzles and $M_j=[0.6...0.9]$, frequency is filtered from $\Delta f=24.9\text{Hz}$ narrowband resolution.

The artanh-function contains suitable properties for continuous fitting. Any polynomial fit with boundary conditions (e.g. polyfix-function) does the job, too.

For a cross-comparison to large scale test data, the $\max(X)=7 \cdot D_j$ source distribution is extracted in Eqn. 1:

$$\frac{X}{D} = 3.5 (\tanh(-2.22(\lg(Sr) - 0.15)) + 1) \quad [-] \quad (1)$$

There is already a good low frequency collapse when just assuming a point source at $\max(X)$, albeit with some deficits. But, the high-frequency parts of the spectra improve when taking the source distribution into account.

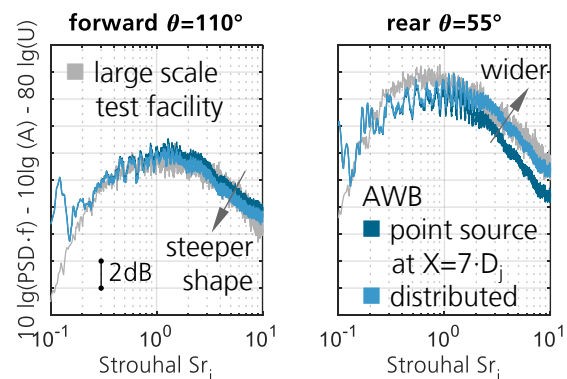


Figure 6: AWB small scale vs. large scale test data, $M_j=0.9$.

Test rig quality

Corrected far-field data is subject to the following metric [3]: For each polar angle Θ , there is an individual spectral shape function \mathcal{F} and an individual velocity exponent n . The shape function and the exponent depend on a temperature ratio TR , for the cold jets at AWB either on the total $TR T_{ij}/T_0=1$ (unheated air), or static $TR T_j/T_0=1$ (isothermal air):

$$I(Sr_j, \theta, TR) \propto \mathcal{F}(Sr_j, \theta, TR) \cdot \left(\frac{U_j}{a_0}\right)^{n(\theta, TR)} \quad [\text{dB}] \quad (2)$$

The scalability of nozzle diameter D_j and microphone distance R is implicitly assumed. The selected velocity parameter is the acoustic Mach number and the dimensionless frequency is the Strouhal number of the jet velocity.

At $R/D_j=100$, the source distribution along the axis can be simplified as "point-like in the nozzle outlet". This very focus on $X=0 \cdot D_j$ instead of the peak SPL position, e.g. $X=7 \cdot D_j$, causes a geometrical error of max. $\pm 0.5\text{dB}$ (in gain, esp. in the rear) and of max. $\pm 2^\circ$ (in polar angle, esp. at overhead). These are the error margins which are deemed negligible in conventional large scale testing.

The AWB data ($R/D_j < 100$) focusses on the low-frequency source point (assumed at $X=7 \cdot D_j$) due to violation of the conventional far-field condition.

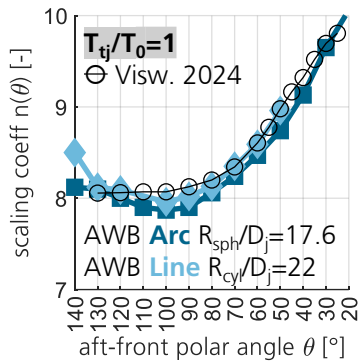


Figure 7: Velocity scaling exponents by polar angle for Ø80mm jet, unheated air.

Jet noise data is validated according to [3] by using multiple jet velocities (here: 6) and nozzle sizes (here 3). The current collapse for the normalized overall sound pressure level, $\text{OASPL} - 10\lg(A_j) - n(\Theta) \cdot 10\lg(U_j)$, is in a band of 4dB for AWB data (Figure 8).

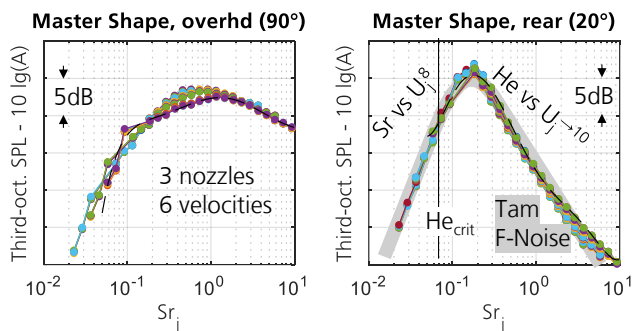


Figure 8: Master-shape function for overhead angles (G-noise) and for rear-arc angles (F-noise)

Test rig build studies

The rig was checked for internal and external rig noise. Instead of a simple "global" quality assessment with $\text{OASPL} - \log(U_j)$, similarity spectra were examined with the criterion $Sr_j < 10$. Hence, small deviations can be detected which are otherwise insignificant to OASPL .

Internal test rig noise was determined by studying a build with and without turbulence screens (Figure 9). The multi-stage cascade improves the similarity of velocity spectra ($\hat{U}/\bar{U}(Re_j)=\text{const.}$ [5]) over a broader range of Mach numbers. This improves the overall broadband accuracy especially for low jet speed jets. Yet, it can be accompanied by additional high-frequency noise (e.g. at $Sr=8 \dots 24$ for $M_j=0.3$). The effect of turbulence screens is unproblematic for $M_j \geq 0.4$.

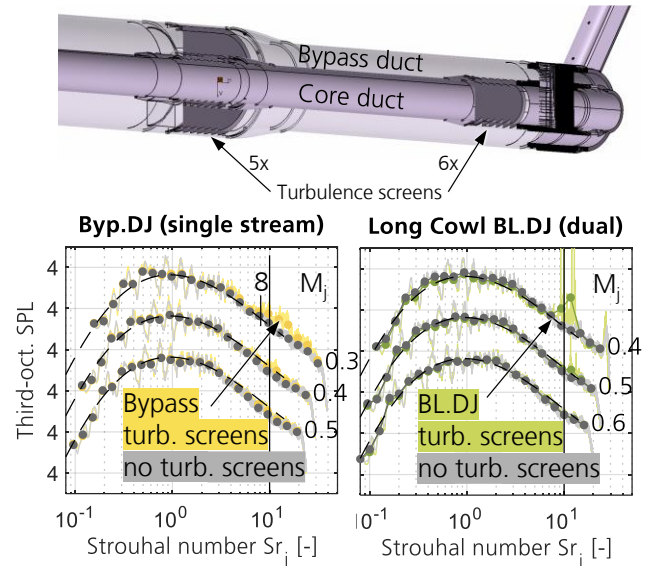


Figure 9: Turbulence screen installation effect for bypass single stream and dual stream flow, staggered plot with 4dB offsets.

External test rig noise was identified at $f=400\text{Hz}$ and 500Hz by changing the vertical collector position (Figure 10). Smaller distances between the engine axis and the collector's foam wall reduce the one-third octave frequencies of $f=400\text{Hz}$ and 500Hz by up to 3dB. The source maps show a shift of the rig noise peak to higher frequencies, which correlates well with spatially compressed jet dimensions.

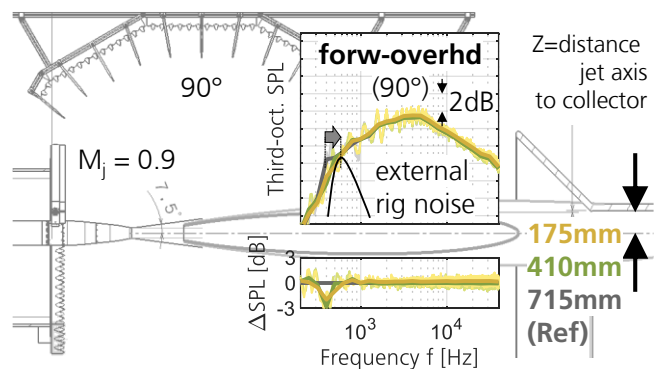


Figure 10: Identification of external rig noise by changing the collector height, $M_j=0.9$.

At slightly higher frequency, the external rig noise seems to lose significance against the higher jet noise signal in the 630Hz frequency band.

Summary and Outlook

Tests in small facilities can deliver useful far-field results, as this example of a static jet noise test of a Ø80mm at AWB has shown. The AWB operation limits are depicted in Figure 11.

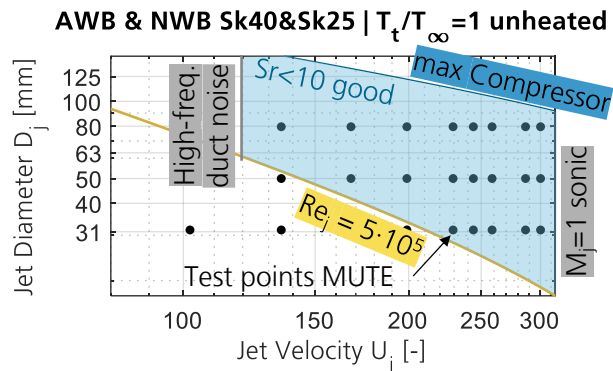


Figure 11: Operating limits for jet noise in the AWB and MUTE operating points

Large scale tests come with the convenience of being able to neglect the exact source position. In order to make small scale tests work, the following points need to be addressed:

The microphone position (polar angle) of the jet noise source is typically not known prior to the test, yet assuming a position downstream the engine axis, i.e. $X=7 \cdot D_j$ (instead of $X=0 \cdot D_j$) is a good start.

Source localization then provides the correct measurement reference point as well as the source distribution. It is optional to use literature for the source distribution of ordinary/common engine models.

An array in the 90° position will address source distributions for most isolated and installed problems in the forward-overhead position. Rear-arc phenomena may require an additional rear-arc array.

The measured low-frequency reference is not a point, but distributed along $\Delta X=3 \cdot D_j$. Therefore, microphones should be well-distanced to it.

The test data might benefit, if entire microphone arcs can be slightly moved by $\pm 1 \cdot D_j$ in X. This would address the slight shift in source position depending on jet Mach number.

Acknowledgements

The author wants to acknowledge the roles of the entire AWB test team as well as the project partners from Rolls Royce Deutschland for conducting the wind tunnel test.

The presented work was funded by the German Federal Ministry for Economic Affairs and Climate Action, as part of the LuFo VI research project MUTE under grant agreement No. 20T1915D.

Literature

- [1] Viswanathan K.: Best Practices for Accurate Measurement of Pure Jet Noise. *International Journal of Aeroacoustics*. 2010; 9(1-2): 145-206. DOI: 10.1260/1475-472X.9.1-2.145, see p.203
- [2] Jente, C., Siller, H., Christophe, J., Lawrence, J.: Isolated jet noise cross-comparison in various EU small and mid-size test facilities and geometric far-field. The DJINN-ENODISE conference, 2023-11, Berlin, Germany. <https://elib.dlr.de/199634/>
- [3] Viswanathan K.: Characteristics of jet noise: A synthesis. *International Journal of Aeroacoustics*. 2024;23(3-4):184-284. DOI: 10.1177/1475472X241230653
- [4] Tam, C. K. W.: "A phenomenological approach to jet noise: the two-source model," *Philosophical Transactions of the Royal Society A: Mathematical, Physical and Engineering Sciences*, Vol. 377, No. 2159, 2019, DOI: 10.1098/rsta.2019.0078
- [5] Yamamoto, K., Arndt, R.: Peak Strouhal frequency of subsonic jet noise as a function of Reynolds number, AIAA, 1979, Williamsburg, Virginia, U.S.A. DOI: 10.2514/6.1979-1525
- [6] Viswanathan, K.: Investigation of the Sources of Jet Noise. 13th AIAA/CEAS Conference, Rome, Italy, 2007. DOI: 10.2514/6.2007-3601, p.7, Figs. 4-5
- [7] Jente, C., Huber, J., Renard, F., Goffredi, T., Paladini, E.: Jet-Flap Installation noise of Pylon Mounted Jet Engine on 3D wing, 30th AIAA/CEAS Conference, Rome, Italy, 2024. DOI: 10.2514/6.2024-3309